Scale-Dependent Properties of Optimal Perturbations on a Zonally Varying Barotropic Flow

HUEI-PING HUANG*

Department of Atmospheric Sciences, University of Illinois, Urbana–Champaign, Urbana, Illinois

ABSTRACT

The scale-dependent characteristics of the optimal perturbations in a zonally asymmetric barotropic model are examined. The dependence of the optimal energy growth on the initial scale is investigated through the calculations of spectrally constrained optimal perturbations. Considering an optimization time of $\tau = 3$ days, and a basic state containing an idealized Asian jet, the optimal amplification factor generally increases with the decrease of the imposed initial scale. In the absence of diffusion, the most amplifying scale becomes the smallest scale in the model. An energetics analysis shows that the energy conversion in the optimal excitation process is dominated by the shear straining term, with a sharp increase in the scale of the perturbation accompanying the explosive energy growth. These results show the similarity between the optimally growing process in the zonally asymmetric system and the shear straining process in a parallel shear flow. Except when a small τ is considered or a sufficiently strong diffusion is used in the system, the optimal energy growth for small-scale disturbances sensitively depends on the zonally varying feature of the basic state. With $\tau = 3$ days, the optimal amplification factors for small-scale disturbances are reduced significantly when the idealized Asian jet is shortened by only one-fifth. At the same time, those for medium- and large-scale disturbances are almost unaffected by the change of the basic state. The reasons for this contrast of the sensitivity property between the small and large scales are discussed.

1. Introduction

Most dynamical systems governing the perturbation motion in the atmosphere are non-self-adjoint. The explosive transient (nonmodal) instability in such systems has recently attracted significant attention from meteorologists. Its characteristics have been investigated in problems related to explosive cyclogenesis (e.g., Farrell 1989a), predictability in numerical weather prediction models (e.g., Molteni and Palmer 1993), and large-scale dynamics (e.g., Farrell 1989b; Borges and Hartmann 1992; Buizza and Palmer 1995). In these studies, the concept of a finite-time ''optimal excitation process'' (Farrell 1988; Lacarra and Talagrand 1988) was developed, with the pair of the optimal perturbation (or ''singular vector'') at day 0 and its day τ counterpart elegantly representing the characteristics of the transient instability.

Although many early studies considered systems with a zonal-flow basic state, interest in the transient instability of a zonally asymmetric basic flow has grown. In their study of the barotropic instability of the large-scale circulation, Borges and Hartmann (1992) showed that the transient instability for the leading optimal perturbations of a zonally asymmetric time-mean flow is much stronger than the normal mode instability. They suggested that low-frequency variability could be efficiently generated by the transient instability of a few leading optimal perturbations, a revision of the original paradigm by Simmons, Wallace, and Branstator (Simmons et al. 1983), which emphasized the importance of a zonally asymmetric basic state but otherwise focused on normal mode instability. Chang and Mak (1995) calculated the optimal perturbations for the 500-mb mean flow in selected winters. On the one hand, they found, as in Borges and Hartmann, that the transient energy growth for the leading optimal perturbations is much stronger than the leading normal modes. On the other hand, they showed that the projections of the observed anomaly field on the leading optimal initial conditions are usually small. In a systematic examination of multiwinter upper-troposphere data, Sardeshmukh et al. (1997) further showed that the potential for the optimal transient (barotropic) instability (for a seasonal mean flow) is seldom realized in the atmosphere.

* Current affiliation: Cooperative Institute for Research in Environmental Sciences, University of Colorado, Boulder, Colorado.

Corresponding author address: Dr. Huei-Ping Huang, NOAA–CIRES Climate Diagnostics Center, University of Colorado, Campus Box 216, Boulder, CO 80309-0216.
E-mail: hp@cdc.noaa.gov

Although the results in the aforementioned studies are not in favor of the Borges–Hartmann picture, one has to note that the definition of the optimal perturbation depends on the problem that is being solved. One may refine the optimal perturbation by imposing constraints on the initial condition, either in the physical or spectral space [see, e.g., Buizza (1994) and Hartmann et al. (1995) for general discussions]. These constraints, which have not been extensively used in previous studies on low-frequency variability, are not without a physical basis. Naturally recurring or externally forced "initial" disturbances in the large-scale circulation may possess a particular spatial scale. In fact, in some classic barotropic model simulations of the global circulation, for example, Basdevant et al. (1981), the effect of high-frequency eddies on the large-scale flow was parameterized as random stirring on the disturbances within a spectral band. The characteristics of the constrained optimal perturbation have not been examined in detail for the transient barotropic instability of a large-scale, zonally asymmetric flow. The purpose of this paper is twofold. First, we investigate the characteristics of the spectrally constrained optimal perturbations for a zonally asymmetric basic state. The dependence of the optimal amplification factor on the imposed initial scale is demonstrated. Second, through the use of constrained optimal perturbation, we discuss the role of the zonal asymmetry of the basic state in the optimal transient instability.

Section 2 presents the procedure that allows the use of an arbitrary combination of spherical harmonics to construct the optimal initial condition for a global barotropic model. Examples of the constrained optimal perturbations, under an idealized zonally asymmetric basic state and a 3-day optimization time, are shown in section 3. When the idealized jet in the basic state is set to resemble the wintertime Asian jet, the constrained optimal amplification factor generally increases with the decrease of the imposed initial scale for the perturbation (unless scale-selective diffusion is imposed to counter this trend). In the inviscid case, the most amplifying scale becomes the smallest scale in the model. In section 4, an energetics analysis shows that the energy conversion in the optimally growing processes is dominated by the shear straining term $[C_y \approx -(uv)\partial\overline{u}/\partial y]$ and not by the deformation term $[C_x \approx -(u^2 - v^2)\partial\overline{u}/\partial x]$. The similarity between the optimally growing process in the zonally asymmetric system and the shear straining process in a parallel shear flow is demonstrated.

In section 5 we discuss the impact of the zonal asymmetry of the basic state on the optimal transient instability. Interestingly, under a 3-day optimization time, shortening the idealized Asian jet by only 20% leads to significant suppression of the (otherwise strong) optimal energy growth for small-scale initial perturbations. In contrast to that, the optimal amplification factors for the medium- and large-scale initial perturbations remain almost the same. We point out that in a zonally asymmetric

flow the ability for a disturbance to grow depends not only on how efficiently it extracts energy from the mean shear $\partial\overline{u}/\partial y,$ but also on how long it stays in the maximum shear zone. A simple estimate based on Rossby wave phase speed and mean flow advection shows that small-scale disturbances move downstream (away from the jet core) much faster than medium- and large-scale ones. Thus, unless a sufficiently short optimization time is used, the optimal amplification factors for small-scale perturbations sensitively depend on the longitudinal extent of the jet. Conclusions and further remarks follow in section 6.

2. Spectrally constrained optimal perturbation

The general procedures for solving the optimization problem have been discussed in many papers, for example, Farrell (1989a) and Borges and Hartmann (1992) for a medium-sized system and Buizza et al. (1993) for a large system. Strategies for constructing constrained (spatially or spectrally localized) optimal perturbations in a large three-dimensional model have also been discussed by Buizza (1994), Hartmann et al. (1995), and Ehrenderfer and Errico (1995). In this work, direct matrix eigenvalue solutions are sought for the barotropic system with a moderate number of degrees of freedom.

The linearized global barotropic model with a zonally asymmetric basic state is (where ψ and ζ are the perturbation streamfunction and vorticity, and f the Coriolis parameter)

$$\frac{\partial\zeta}{\partial t} = -J(\psi, \nabla^2\Psi + f) - J(\Psi, \zeta) - \gamma\nabla^4\zeta. \quad (1)$$

The basic-state streamfunction Ψ, which contains an idealized jet in the Northern Hemisphere resembling the wintertime Asian jet, is shown in the background of Figs. 1 and 2. Both viscous and inviscid ($\gamma = 0$) cases are discussed. A triangular 26 spectral truncation is used, with a total of 727 degrees of freedom. For more details of the model and the basic state, see Huang and Robinson (1995). The spectral form of the system in (1) can be written as

$$\frac{d\zeta}{dt} = \mathbf{L}\zeta, \quad (2)$$

where $\mathbf{L}$ is a linear operator, and ζ the state vector containing the spherical harmonic coefficients of the perturbation vorticity. The system can always be arranged in real variables (e.g., Chang and Mak 1995), as adopted in this work. The solution of (2) at time τ can be related to the initial condition by a linear relationship, $\zeta(\tau) = \mathbf{G}(\tau)\zeta(0)$. In the unconstrained problem $\mathbf{G}$ is an $N \times N$ matrix, with N the total number of degrees of freedom. Since the general solution of (2) is $\zeta(\tau) = \exp(\mathbf{L}\tau)\zeta(0)$, in some work the operator $\mathbf{G}(\tau)$ is constructed by a careful evaluation of the Taylor expansion of the matrix exponential function $\exp(\mathbf{L}\tau)$ (Molteni and Palmer
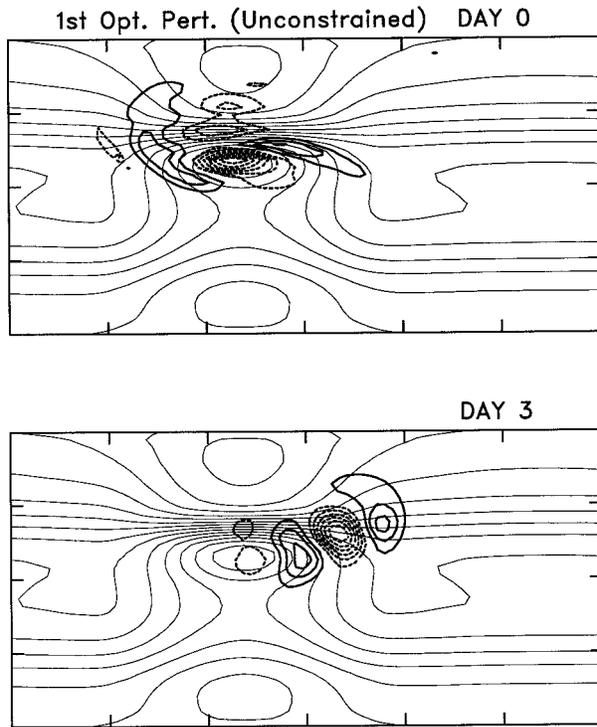
FIG. 1. The streamfunctions for the first viscous, unconstrained 3-day optimal perturbation at day 0 (upper) and day 3 (lower). The amplification factor has been removed from the day-3 picture. The light contours in the background show the streamfunction of the basic state. The domain is global.
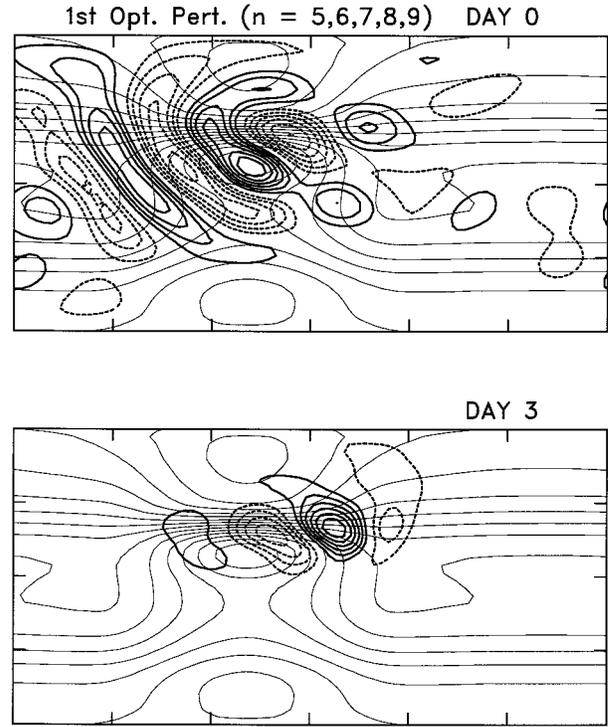
FIG. 2. Same as Fig. 1 but for the first viscous, constrained 3-day optimal perturbation with the initial condition restricted to $n = 5, 6, 7, 8, 9$.

1993). Two other convenient (when N is not large) and precise methods are (i) generating $\mathbf{G}(\tau)$ by using the whole set of normal modes (e.g., Farrell 1989b; Borges and Hartmann 1992) and (ii) constructing $\mathbf{G}(\tau)$ column by column by integrating (2) N times, starting with N orthogonal initial perturbations [Lorenz (1965); see Chen et al. (1997) for a recent application]. In the global barotropic model we perturb spherical harmonics one at a time. The calculations in this work rely mainly on method ii. To provide an independent check, a computer code based on method i is also created. The two procedures produce identical results.

Consider the spectrally constrained case in which only M selected spherical harmonic components are allowed in the initial condition. The M-element restricted initial condition is denoted by $\tilde{\boldsymbol{\zeta}}(0)$. With $M \leq N$, the later-time development $\boldsymbol{\zeta}(\tau)$ can still contain all N components. The two vectors $\boldsymbol{\zeta}(\tau)$ and $\tilde{\boldsymbol{\zeta}}(0)$ are now related by $\boldsymbol{\zeta}(\tau) = \tilde{\mathbf{G}}(\tau)\tilde{\boldsymbol{\zeta}}(0)$, where $\tilde{\mathbf{G}}(\tau)$ is an $N \times M$ matrix that can be obtained by integrating (2) M times or readily deduced from $\mathbf{G}(\tau)$ by trimming the irrelevant columns. For the constrained system, the energies at $t = 0$ and τ are $E(0) = \tilde{\boldsymbol{\zeta}}(0)^{\mathrm{T}}\tilde{\mathbf{D}}\tilde{\boldsymbol{\zeta}}(0)$ and $E(\tau) = \tilde{\boldsymbol{\zeta}}(0)^{\mathrm{T}}\tilde{\mathbf{G}}(\tau)^{\mathrm{T}}\mathbf{D}\tilde{\mathbf{G}}(\tau)\tilde{\boldsymbol{\zeta}}(0)$; $\mathbf{D}$ is an $N \times N$ diagonal matrix representing the ∇^{-2} operator; the superscript "T" denotes transpose, and the $M \times M$ matrix $\tilde{\mathbf{D}}$ is the part of $\mathbf{D}$ corresponding to

the nonzero spherical harmonic components in the initial condition. The ratio between $E(\tau)$ and $E(0)$, $\lambda = E(\tau)/E(0)$, is the constrained amplification factor. Optimization of λ, by requiring $\partial\lambda/\partial\tilde{\zeta}_i = 0$ ($i = 1, 2, \ldots, M$), leads to an $M \times M$ eigenvalue problem

$$\underset{M \times M}{\tilde{\mathbf{H}}(\tau)}\tilde{\boldsymbol{\zeta}}(0) = \lambda\tilde{\mathbf{D}}\tilde{\boldsymbol{\zeta}}(0), \qquad \underset{M \times M}{\tilde{\mathbf{H}}(\tau)} \equiv \underset{M \times N}{\tilde{\mathbf{G}}(\tau)^{\mathrm{T}}} \underset{N \times N}{\mathbf{D}} \underset{N \times M}{\tilde{\mathbf{G}}(\tau)}. \quad (3)$$

The eigenvectors of (3) are the constrained optimal perturbations and the corresponding eigenvalues their amplification factors. The eigenvectors satisfy the orthogonal relationship $\tilde{\boldsymbol{\zeta}}_i(0)^{\mathrm{T}}\tilde{\mathbf{D}}\tilde{\boldsymbol{\zeta}}_j(0) = E_i(0)\delta_{ij}$, and their day-$\tau$ counterparts $\boldsymbol{\zeta}_i(\tau)^{\mathrm{T}}\mathbf{D}\boldsymbol{\zeta}_j(\tau) = E_i(\tau)\delta_{ij}$, with $E_i(\tau) = \lambda_i E_i(0)$.

3. Dependence of the optimal amplification factor on the initial scale

Figure 1 shows the streamfunctions of the first unconstrained 3-day optimal perturbation of the barotropic system, at day 0 and day 3, under a diffusion coefficient $\gamma = 2 \times 10^{16} \mathrm{~m}^4 \mathrm{~s}^{-1}$. The basic-state streamfunction is shown as the thin contours in the background. The domain is global. The optimal eigenvectors are solved using (3) with $M = N$. The energy amplification factor for the first optimal perturbation is 18.8, far exceeding that of the most unstable normal mode, whose phase-averaged amplification factor is only 1.7 in 3 days [see Huang and Robinson (1995) for details of the normal mode]. A few of the higher optimal eigenvectors also

have amplification factors much greater than the most unstable normal mode (e.g., 17.2 for the second eigenvector; 11.3 for the third). Their structures and dynamical properties are similar to those of the first optimal perturbation. In the following we will focus on the first eigenvector. Figure 2 shows the first 3-day, spectrally constrained optimal perturbation, with its initial condition restricted to the spherical harmonic components Y_n^m with total wavenumbers $n = 5, 6, 7, 8, 9$, excluding the zonal components ($m = 0$). Figures 1 and 2 share some common characteristics. The day-0 patterns show a wave train tilting against the maximum meridional shear. The tilting is reduced at day 3, with the amplified disturbance appearing downstream of the jet center. (For clarity, in Figs. 1 and 2 the amplification factors have been removed from the day-3 pattern.) The constrained case has a much smaller amplification factor of 5.5, although it is still greater than that of the most unstable normal mode.

To explore the dependence of the optimal amplification factor on the imposed initial scale, calculations similar to the case in Fig. 2 are performed under different $\overline{n}$, the center of a spectral "band" consisting of five total wavenumbers, $\overline{n} - 2$, $\overline{n} - 1$, $\overline{n}$, $\overline{n} + 1$, and $\overline{n} + 2$ (see Fig. 3c). The amplification factors for the first 3-day constrained optimal perturbations, under a diffusion coefficient $\gamma = 2 \times 10^{16}$ m^4 s^{-1}, are shown in Fig. 3a as the open circles. Three-band (with $n = \overline{n} - 1$, $\overline{n}$, and $\overline{n} + 1$) and seven-band calculations are also performed, with their amplification factor curves (not shown) below and above the five-band case. Otherwise, the three cases show similar qualitative trends. In Fig. 3a the open-circle (viscous) curve peaks at around $\overline{n} = 15$–17, close to the mean total wavenumber of the first unconstrained optimal initial condition. This peak shifts toward smaller scales with reduced diffusion (not shown). On the low wavenumber side, the viscous curve declines toward the large scales, with a sharp drop after $\overline{n} < 7$, reflecting that very large-scale disturbances "feel" little influence of the shear and deformation associated with the jet in the basic state. The decline of the amplification factors toward the small-scale side with $\overline{n} > 17$ is due to the increasing strength of diffusion. This can be seen by repeating the above calculations for the inviscid case ($\gamma = 0$). The results are shown in Fig. 3a as the cross circles. The amplification factors for the inviscid case (and cases with weak diffusion; not shown) increase monotonically toward small scales. In section 5 we will show, however, that in these cases the optimal amplification factors for the small-scale disturbances sensitively depend on the zonally varying characteristics of the basic state in the barotropic model.

We have so far used the total wavenumber n to define the scale. It is perhaps the most useful choice, since most global models use a Laplacian-type diffusion that depends on the total wavenumber. Another interesting choice is to define the scale by the meridional wave-

number $J = n - m$. The use of J is motivated by the fact that, in the classic Orr problem for a simple parallel shear flow, the explosive transient energy growth is associated with a decaying meridional wavenumber and a conservative zonal wavenumber for the perturbation. Thus, J could be a more straightforward index than n to characterize the process. Figure 3b is similar to the inviscid case in Fig. 3a but with the spectral constraints imposed on J. Each $\overline{J}$ in Fig. 3b represents five spectral bands as shown in Fig. 3c. Similar to Fig. 3a, the amplification factors in Fig. 3b also show a monotonic increase toward small scales.

4. Energetics of the optimally growing processes

To show further the nature of the optimally growing process, an energetics analysis is performed. The globally integrated energy equation for system (1) can be written as (with the angle brackets denoting the global integral)

$$\frac{\partial E}{\partial t} = \langle C \rangle + \langle D \rangle, \qquad (4)$$

where E is the globally integrated perturbation energy, and C the energy conversion term with

$$C = C_x + C_y,$$

$$C_x = -(u^2 - v^2)\left[\frac{1}{a\cos\theta}\frac{\partial \overline{u}}{\partial \lambda} - \frac{\overline{v}}{a}\tan\theta\right],$$

$$C_y = -(uv)\left[\frac{1}{a\cos\theta}\frac{\partial \overline{v}}{\partial \lambda} + \frac{1}{a}\frac{\partial \overline{u}}{\partial \theta} + \frac{\overline{u}}{a}\tan\theta\right]. \qquad (5)$$

The (u, v) and $(\overline{u}, \overline{v})$ are the perturbation and basic-state velocities, and θ and λ are latitude and longitude. The C_x and C_y, the "deformation" and "shear straining" terms, are usually dominated by their first and second terms, respectively [they are sometimes approximated by $C_x \approx -(u^2 - v^2)\partial\overline{u}/\partial x$ and $C_y \approx -(uv)\partial\overline{u}/\partial y$]. The "positive conversion" phase of C_x is characterized by a zonally elongated eddy straddling the jet exit, while that of C_y is a wave train tilting against the meridional shear of the zonal wind in the region with maximum shear [for a detailed discussion of the energetics, see Simmons et al. (1993); Hoskins et al. (1983); and Mak and Cai (1989)]. The D term in (4) is the energy dissipation caused by diffusion. It can be calculated as $D = \mathbf{v} \cdot \mathbf{F}$, with $\mathbf{v} = (u, v)$ and $\mathbf{F} = -\gamma\mathbf{z} \times \nabla(\nabla^2\zeta)$ ($\mathbf{z}$ is the outward unit normal vector of the earth's surface). To preserve numerical accuracy, the energetics calculations are performed under a higher spectral resolution and corresponding high-resolution Gaussian grids using the spectral transform method, as in Huang and Robinson (1995).

Figure 4a shows the time evolution of the *growth rates* (the conversion term divided by the perturbation energy) associated with the conversion and diffusion
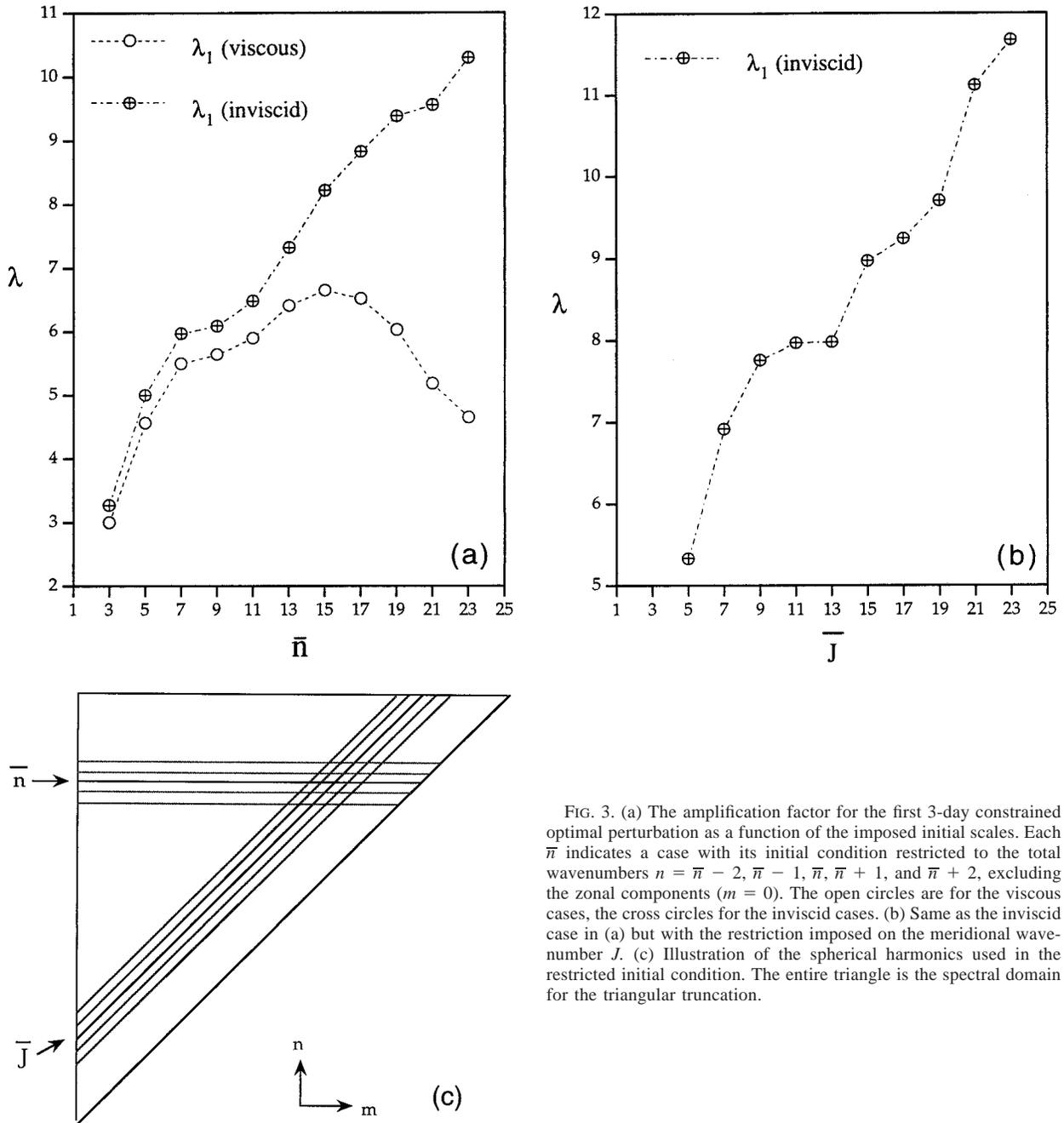
FIG. 3. (a) The amplification factor for the first 3-day constrained optimal perturbation as a function of the imposed initial scales. Each $\overline{n}$ indicates a case with its initial condition restricted to the total wavenumbers $n = \overline{n} - 2$, $\overline{n} - 1$, $\overline{n}$, $\overline{n} + 1$, and $\overline{n} + 2$, excluding the zonal components ($m = 0$). The open circles are for the viscous cases, the cross circles for the inviscid cases. (b) Same as the inviscid case in (a) but with the restriction imposed on the meridional wavenumber J. (c) Illustration of the spherical harmonics used in the restricted initial condition. The entire triangle is the spectral domain for the triangular truncation.

terms in a linear initial value problem, starting with the first 3-day unconstrained optimal initial condition for the viscous case. The diffusion term is negligible except at the beginning (see below for explanation). The large transient energy growth within 3 days is contributed primarily by the C_y (shear straining) term, whose growth rate peaks before day 3. The negative C_x at day 3 is consistent with the day-3 pattern in Fig. 1, which shows a slightly meridionally elongated eddy in the jet exit.

To highlight the signature of the shear straining pro-cess in the transient instability of the zonally asymmetric system, we consider the following characteristics of the classic shear straining process for a simple parallel shear flow (e.g., Boyd 1983; Tung 1983; Shepherd 1985). During the growing phase the perturbation enstrophy H is conserved while the energy E increases. Thus, (the square root of) their ratio, $(H/E)^{1/2}$, the mean total wave-number, decreases. Figure 4b shows the time evolution of the mean total wavenumber $[H(t)/E(t)]^{1/2}$ correspond-ing to the process shown in Fig. 4a. [Note that in the
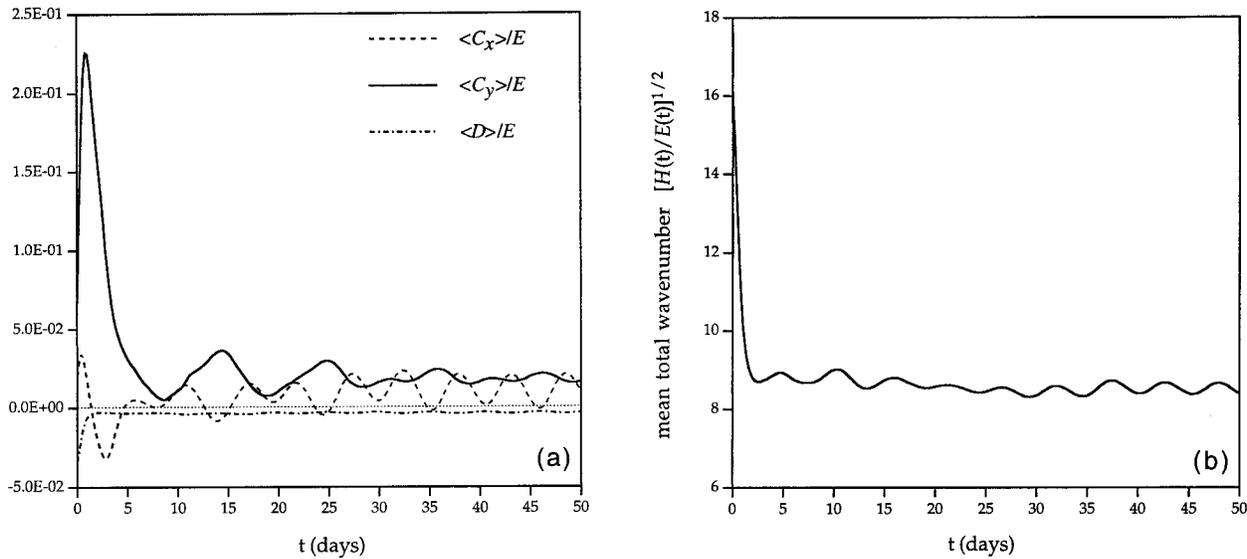
FIG. 4. (a) The time evolution of the energy growth rates associated with the conversion and diffusion terms for the initial value problem starting with the first viscous, unconstrained 3-day optimal perturbation. The dashed, solid, and dot–dashed curves are for the C_x, C_y, and D terms defined in the text. (b) The time evolution of the mean total wavenumber corresponding to the process shown in (a).

global barotropic model H/E represents the mean value of the quantity $n(n + 1)$.] A sharp initial decline of the total wavenumber (initially at $n \approx 15$–20), associated with the fastest growing phase, is clearly seen. At large times the disturbances evolve into the most unstable normal mode. (Note that the curves in Figs. 4a and 4b exhibit periodic behavior at large times.) For the leading normal mode the energy conversions are weaker and the magnitudes of the C_x and C_y terms are comparable. [The "positive C_x picture" of a zonally elongated eddy straddling the jet exit is seen in one phase of the most unstable normal mode; see Huang and Robinson (1995).] The scale of the most unstable normal mode oscillates around $\overline{n} \approx 8$, as can be seen in Fig. 4b.

The pictures for the energetics and the evolution of scales in Fig. 4 are also commonly seen in the constrained optimal perturbations. Figure 5 is similar to Fig. 4a but uses the first inviscid, constrained 3-day optimal perturbations, with $\overline{n} = 7$ and 19, as the initial conditions. Even in the (relatively) moderately growing case with $\overline{n} = 7$, the C_y term dominates during the explosively growing stage. In general, it is the strong shear straining process that makes the optimal perturbations grow much faster than the leading normal mode.

Consistent with the picture of the classic shear straining process, while the smallest scales perform strongly in the constrained *energy* optimization problem, they do much less impressively in the *enstrophy* optimization problem. (Note that enstrophy is conserved in the shear straining process with a constant shear.) When energy is replaced by enstrophy for optimization, the first 3-day constrained optimal perturbation for the inviscid, $\overline{n} = 23$ case has an amplification factor of only 2.84, compared with 10.3 for its counterpart with energy opti-

mization. The structure of the enstrophy-optimal initial perturbation is also different from the energy-optimal one. For example, in the unconstrained case the streamfunction field of the former possesses a much larger spatial scale than the latter.

5. The impact of the zonal asymmetry of the basic state

Since the leading optimal perturbations in our system obtain their energy primarily through the shear straining process similar to the classic Orr process in a parallel shear flow, one may ask if the zonal asymmetry of the basic state has any impact on the optimal transient instability. The answer is yes. We use a sensitivity test to illustrate the point. Figure 6 shows five different basic states (with only part of the Northern Hemisphere shown), with case I corresponding to the standard case used before. The cases II–V are similarly constructed as case I [see Huang and Robinson (1995) for details] but with the length of the jet $L_J = 0.9$, 0.8, 0.75, and 0.66 L_O; L_O is the length of the jet in case I. The meridional profiles at the jet center are the same for the five cases. They are also the same far downstream or upstream of the jet center. Each of the cases II–V possesses a shorter "high shear zone" (with large $\partial \overline{u}/\partial y$) than case I. The $\partial \overline{u}/\partial x$ term (averaged from jet core to jet exit) is smaller for the latter. As discussed in section 4, however, this term is less important to the energetics of the optimally growing processes.

Figure 7a shows the amplification factors for the first inviscid, constrained 3-day optimal perturbations under the five basic states. Similar to Fig. 3a, each point in the figure is for a five-band spectrally constrained initial
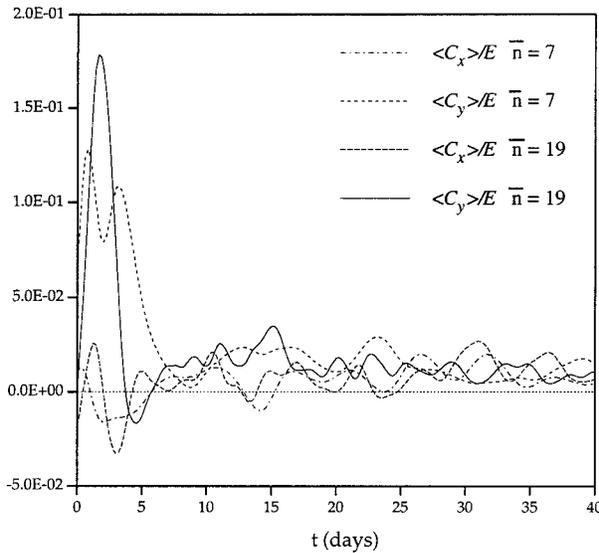
FIG. 5. Same as Fig. 4a but for the two inviscid, constrained cases, with $\overline{n} = 7$ and 19, as the initial conditions. The dot–dashed and short dashed curves are for C_x and C_y with $\overline{n} = 7$; long dashed and solid curves for C_x and C_y with $\overline{n} = 19$. The D term is zero for the inviscid case.

FIG. 6. The five basic states for the cases I–V used in the sensitivity experiment. Only part of the Northern Hemisphere is shown.

condition. As shown in Fig. 7a, one needs to reduce the length of the jet by only 20% to significantly suppress the strongly growing part in small scales (however, the amplification curves eventually go up at the very small-scale end). In contrast to this sensitive dependence on the basic state, the medium- and large-scale (e.g., $n \leq 13$) constrained optimal amplification factors are more robust against the change of the meridional extent of the jet. This difference might be explained by the scale dependence of the propagation speed of Rossby waves. Using a very simple argument, the timescale for a disturbance to travel from the jet center to the jet exit is roughly $T \approx (U + c)^{-1}(L_J/2)$, where U is the mean-flow zonal velocity, c the Rossby phase speed (in the absence of the mean flow), and L_J the longitudinal extent of the jet. In general, small-scale disturbances have small negative (westward) c, or $U + c \approx U$, while medium- and large-scale disturbances are characterized by $|c| \approx U$. {For example, using the Rossby–Haurwitz formula for a spherical harmonic Y_n^m, we have $c = -2[n(n + 1)]^{-1}a\Omega \cos(\theta)$. At $\theta = 30°N$, this gives $c = -26.7$ m s^{-1} for $n = 5$ and -1.9 m s^{-1} for $n = 20$.} With a negligible c, for small-scale disturbances we have $T \approx L_J/(2U)$, which is typically 1–2 days for the standard case I, with $L_J \approx 10^4$ km and $U \approx 30$ m s^{-1}. (The downstream propagation eventually slows down when the disturbances reach the jet exit.) Thus, to achieve large transient growth, small-scale disturbances have to extract substantial amounts of energy from the background shear $\partial \overline{u}/\partial y$ within a very short time. As the jet is shortened, it becomes increasingly difficult for them to do so. Medium- and large-scale disturbances, on the other hand, move away from the jet center more slowly
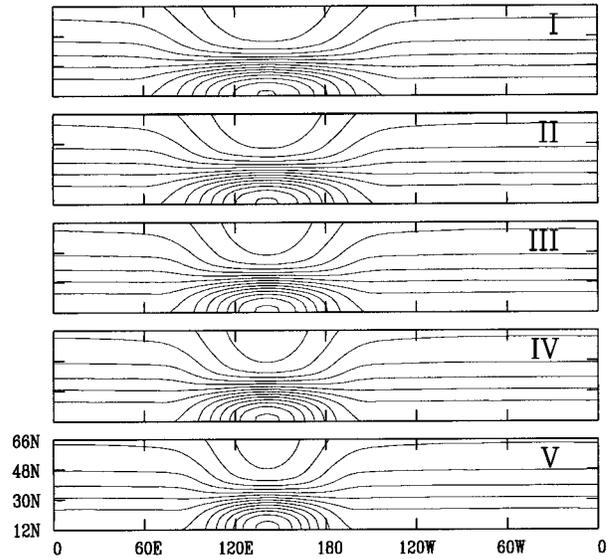
(they have large T), such that they have plenty of time to grow on the maximum meridional shear even with a shortened jet. Thus, their optimal amplification factors are less sensitive to the zonally varying characteristics of the jet.

In the above we have used a simple argument of Rossby phase speed to estimate the timescale for the downstream propagation of a growing disturbance. A more precise argument would involve the group velocity. A discussion in this aspect requires a clear definition of a wave packet and an appropriate spatial averaging of local wavenumbers. Although these complexities are not pursued here, it is useful to comment on the similarity and difference between the phase speed and group velocity. Considering simple plane geometry (and in the absence of a background flow), the Rossby phase speed and group velocity are $c = -\beta/K^2$ and $c_g = \beta(k^2 - l^2)/K^4$, where k, l, and $K = (k^2 + l^2)^{1/2}$ are the zonal, meridional, and total wavenumber, respectively. In our model, the optimal initial perturbation usually shows a significant phase tilt against the meridional shear, with $l^2 > k^2$. On the other hand, an extremely large ratio of l^2/k^2 is not found in the optimal initial condition. (Note that although setting $l^2/k^2 \rightarrow \infty$ in the classic shear straining problem results in an extremely large energy amplification, the time required for the perturbation to reach its maximum energy is also extremely long in that case. In other words, waves with a near 90° phase tilt are not necessarily optimal for energy growth within a *finite* time.) Overall, for a small-scale optimal initial perturbation c_g is also negative and small (compared with the mean flow U). Finally, it has been shown by Tung (1983) that (in a constant shear flow) the energy amplification factor for a wave packet that peaked at (k, l) is similar to that for a plane wave with wave-
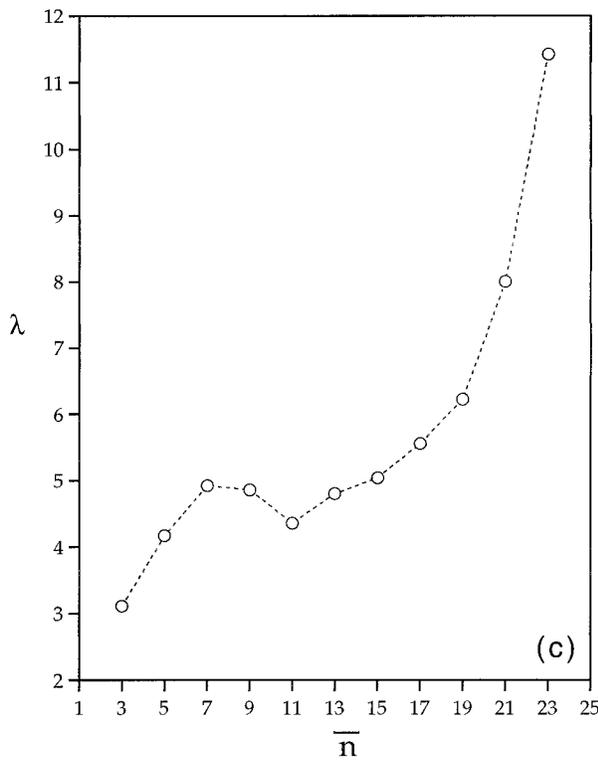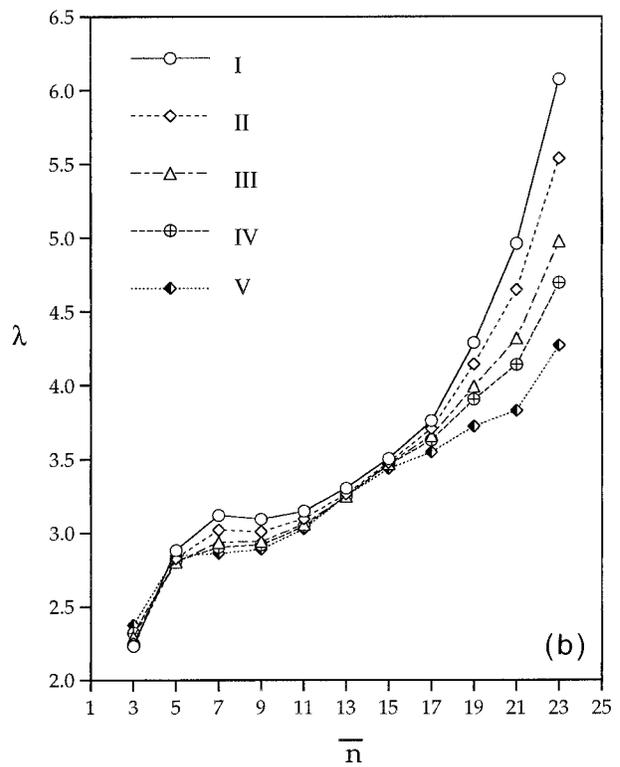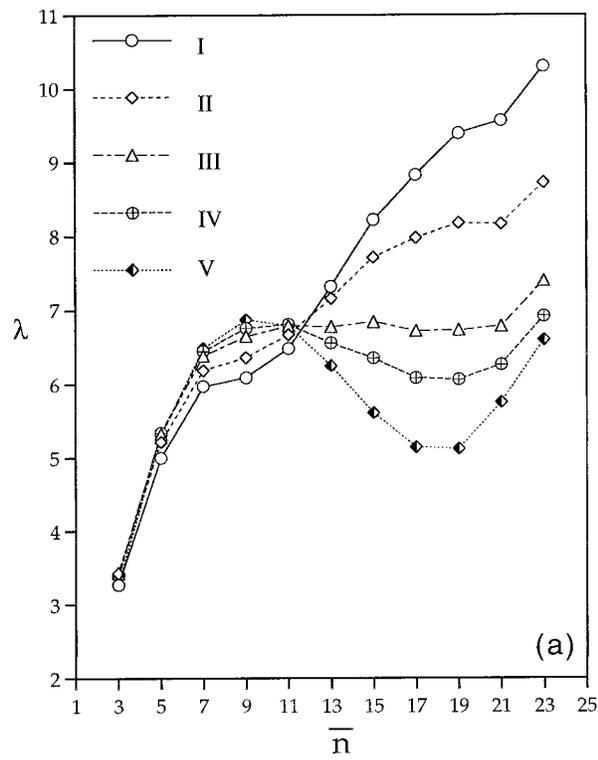
FIG. 7. (a) The amplification factor for the first inviscid, constrained 3-day optimal perturbation as a function of the imposed initial scale $\overline{n}$, for cases I–V. (b) Same as (a) but for 1.5-day optimal perturbations. (c) Same as (b) but with a zonally symmetric basic state (see text for detail).

numbers (k, l). Thus, our previous discussions with plane waves are also relevant to wave packets.

From the above discussion, we expect that if the optimization time τ is reduced to a value comparable to or smaller than the ''downstream propagation'' time T for small-scale disturbances, then the sensitive dependence shown in Fig. 7a should be reduced. (An addition of a diffusion term also reduces the sensitivity, as can be inferred from Fig. 3a.) This is clearly seen in Fig. 7b, in which we choose $\tau = 1.5$ days to repeat the calculations in Fig. 7a. For $\tau = 1$ day (not shown) the amplification factor curves for the five basic states become very close to each other. Since with $\tau \to 0$ the zonally varying feature of the basic state is almost not felt by the optimal perturbations within time τ, the characteristics of the optimal amplification factors in Fig. 7b should be similar to those in a zonally symmetric system, with its basic state constructed from the meridional profiles around the jet center. This is shown in Fig. 7c, which is similar to Fig. 7b but for a zonally symmetric basic state, constructed by zonally averaging the basic state of case I from the jet center to 2500 km downstream of it. In the figure, the tendency of increasing amplification factors toward small scales is very similar to Fig. 7b. (The greater amplification factors in Fig. 7c are expected, since in this case a strong meridional shear extends along an entire latitude circle.)

6. Conclusions and further remarks

In this study we examined several aspects of the spectrally constrained optimal perturbations on a large-scale barotropic jet. Using a basic state with an idealized Asian jet (case I) and an optimization time of 3 days, the amplification factors of the leading constrained optimal perturbations generally increase with decreasing imposed initial scales. In the absence of scale-selective diffusion, the smallest scales in the model become the most amplifying. This result implies that, without sufficiently strong diffusion, the optimal transient growth rate increases with an increasing spectral resolution of the numerical model. This resolution dependence may be reduced by using a diffusion term that is strong enough to suppress the upward trend of the optimal amplification factor in the small-scale end. An example is the dashed (viscous) curve shown in Fig. 3a. Because a diffusion term is used in most general circulation models [dependence of the characteristics of the optimal perturbation on model resolution in these baroclinic models are discussed by Hartmann et al. (1995) and Rabier et al. (1996)], the sensitive dependence shown in our inviscid cases can be considered as the extreme. However, exploring the contrast between the inviscid and viscous cases helps us understand both the nature of the optimal growth and the impact of the scale-selective diffusion.

In the case with weak (or zero) diffusion, the sensitive dependence implies that it is more meaningful to consider the constrained case with the small scales excluded from the initial condition. Use of such a constraint might be justified in some problems related to the generation of large-scale, low-frequency variability, given that in the upper troposphere the observed energy spectrum drops sharply toward small scales. [For example, at the 200-mb level, the transient eddy kinetic energy spectrum $E(n)$ can be roughly described by a power law with $E(n) \propto n^{-3}$ for $14 < n < 25$; see Boer and Shepherd (1983) and Chen and Wiin-Nielsen (1978)]. However, as a reviewer pointed out, an exclusion of small-scale disturbances is not desirable for applications related to the error growth in numerical weather prediction, because in that problem the analysis errors in the initial state could peak at small scales.

An energetics analysis shows that the shear straining term dominates the energy conversion for the optimal transient growth. A sharp decrease in the wavenumber of the perturbation coincides with the fastest growing phase of the optimal excitation process. These results suggest that the optimally growing process in the zonally asymmetric system is similar to the shear straining process in a parallel shear flow. Despite this similarity, the energy amplification factors for the small-scale constrained optimal perturbations sensitively depend on the zonally varying feature of the basic state (although those for the medium- and large-scale optimal disturbances are more robust). This is because small-scale disturbances travel downstream (away from the jet center) much faster than large-scale ones. Thus, their ability to extract substantial amounts of energy from the background shear $\partial \overline{u}/\partial y$ is offset by their inability to stay at the maximum shear zone for a sufficiently long time. The latter factor becomes significant when the jet is shortened from the ''standard'' Asian jet by just one-fifth. This sensitive dependence of the transient growth rate on the zonal asymmetry of the basic state reminds us of Pierrehumbert's (1984) general argument that on a zonally varying mean flow the growth rate for a disturbance is intimately related to its propagation speed (or frequency). While Pierrehumbert (also, Mak and Cai 1989) has focused on the normal mode instability, here we show that this growth rate–frequency dependence is also important for the transient, nonmodal instability. A rigorous theoretical treatment of this interesting aspect is left to future work.

In this work we considered only spectrally constrained optimal perturbations. Another useful choice is to localize the initial condition in physical space in the optimization problem. A general discussion of this aspect can be found in, for example, Buizza (1994). In our global barotropic model, a natural way to construct the spatially constrained optimal perturbation would be to use Lorenz's method (the ''perturbation method'') described in section 2, but with the selected spherical harmonics in the initial condition replaced by selected finite elements S_{ij} [S_{ij} is unity at the grid point (λ_i, θ_j)

and zero elsewhere; see, e.g., Temperton (1991) for a review.]

Recent studies by Borges and Sardeshmukh (1995) and Sardeshmukh et al. (1997) have suggested that internal barotropic dynamics (specifically, the interaction between the anomaly and a barotropic time-mean flow) may not be sufficient to explain the observed extratropical, low-frequency variability, indicating the importance of the role of external forcing. Branstator (1985) has pointed out that strong responses can be excited in a system when a steady external forcing has a significant projection on its adjoint mode, which is the optimal initial perturbation for $\tau = \infty$. Zhang (1988) and Ferranti et al. (1990) have discussed similar ideas. Although determining the precise spatial and temporal pattern of the external forcing is sometimes a difficult task, it is useful to consider the forcing in a statistical sense, in terms of its characteristic scales and the geographical location of its recurrence. Imagine, for example, the effect of forcing as random stirring on a particular scale (or in a particular region); a useful way to assess its impact would be to look at the constrained optimal perturbations with their initial conditions restricted to the forcing scale (or region). An investigation in this direction is suggested for future work.

REFERENCES

Basdevant, C., B. Legras, R. Sardourny, and M. Béland, 1981: A study of barotropic model flows: Intermittency, waves and predictability. *J. Atmos. Sci.,* **38,** 2305–2326.

Boer, G. J., and T. G. Shepherd, 1983: Large-scale two-dimensional turbulence in the atmosphere. *J. Atmos. Sci.,* **40,** 164–184.

Borges, M. D., and D. L. Hartmann, 1992: Barotropic instability and optimal perturbations of observed nonzonal flows. *J. Atmos. Sci.,* **49,** 335–354.

——, and P. D. Sardeshmukh, 1995: Barotropic Rossby wave dynamics of zonally varying upper-level flows during northern winter. *J. Atmos. Sci.,* **52,** 3779–3796.

Boyd, J. P., 1983: The continuous spectrum of linear Couette flow with the beta effect. *J. Atmos. Sci.,* **40,** 2304–2308.

Branstator, G., 1985: Analysis of general circulation model sea-surface temperature anomaly simulations using a linear model. Part II: Eigenanalysis. *J. Atmos. Sci.,* **42,** 2242–2254.

Buizza, R., 1994: Localization of optimal perturbations using a projection operator. *Quart. J. Roy. Meteor. Soc.,* **120,** 1647–1681.

——, and T. N. Palmer, 1995: The singular-vector structure of the atmospheric global circulation. *J. Atmos. Sci.,* **52,** 1434–1456.

——, J. Tribbia, F. Molteni, and T. N. Palmer, 1993: Computation of optimal unstable structures for a numerical weather prediction model. *Tellus,* **45A,** 388–407.

Chang, J.-C. J., and M. Mak, 1995: Nonmodal barotropic dynamics of the intraseasonal disturbances. *J. Atmos. Sci.,* **52,** 896–914.

Chen, T.-C., and A. Wiin-Nielsen, 1978: Non-linear cascades of atmospheric energy and enstrophy in a two-dimensional spectral index. *Tellus,* **30,** 313–322.

Chen, Y.-Q., D. S. Battisti, T. N. Palmer, J. Barsugli, and E. S. Sarachik, 1997: A study of the predictability of tropical Pacific SST in a coupled atmosphere–ocean model using singular vector analysis: The role of the annual cycle and the ENSO cycle. *Mon. Wea. Rev.,* **125,** 831–845.

Ehrendorfer, M., and R. M. Errico, 1995: Mesoscale predictability and the spectrum of optimal perturbations. *J. Atmos. Sci.,* **52,** 3475–3500.

Farrell, B. F., 1988: Optimal excitation of neutral Rossby waves. *J. Atmos. Sci.,* **45,** 163–172.

——, 1989a: Optimal excitation of baroclinic waves. *J. Atmos. Sci.,* **46,** 1193–1206.

——, 1989b: Transient development in confluent and diffluent flows. *J. Atmos. Sci.,* **46,** 3279–3288.

Ferranti, L., T. N. Palmer, F. Molteni, and E. Klinker, 1990: Tropical–extratropical interaction associated with the 30–60 day oscillation and its impact on medium and extended range prediction. *J. Atmos. Sci.,* **47,** 2177–2199.

Hartmann, D. L., R. Buizza, and T. N. Palmer, 1995: Singular vectors: The effect of spatial scale on linear growth of disturbances. *J. Atmos. Sci.,* **52,** 3885–3894.

Hoskins, B. J., I. N. James, and G. H. White, 1983: The shape, propagation and mean-flow interaction of large-scale weather systems. *J. Atmos. Sci.,* **40,** 1595–1612.

Huang, H.-P., and W. A. Robinson, 1995: Barotropic model simulations of the North Pacific retrograde disturbances. *J. Atmos. Sci.,* **52,** 1630–1641.

Lacarra, J.-F., and O. Talagrand, 1988: Short-range evolution of small perturbations in a barotropic model. *Tellus,* **40A,** 81–95.

Lorenz, E. N., 1965: A study of the predictability of a 28-variable atmospheric model. *Tellus,* **17,** 321–333.

Mak, M., and M. Cai, 1989: Local barotropic instability. *J. Atmos. Sci.,* **46,** 3289–3311.

Molteni, F., and T. N. Palmer, 1993: Predictability and finite-time instability of the northern winter circulation. *Quart. J. Roy. Meteor. Soc.,* **119,** 269–298.

Pierrehumbert, R. T., 1984: Local and global baroclinic instability of zonally varying flow. *J. Atmos. Sci.,* **41,** 2141–2162.

Rabier, F., E. Klinker, P. Courtier, and A. Hollingsworth, 1996: Sensitivity of forecast errors to initial conditions. *Quart. J. Roy. Meteor. Soc.,* **122,** 121–150.

Sardeshmukh, P. D., M. Newman, and M. D. Borges, 1997: Free Rossby wave dynamics of the wintertime low-frequency flow. *J. Atmos. Sci.,* **54,** 5–23.

Shepherd, T. G., 1985: Time development of small disturbances to plane Couette flow. *J. Atmos. Sci.,* **42,** 1868–1871.

Simmons, A. J., J. M. Wallace, and G. Branstator, 1983: Barotropic wave propagation and instability, and atmospheric teleconnection patterns. *J. Atmos. Sci.,* **40,** 1363–1392.

Temperton, C., 1991: Finite element method. *Proc. Numerical Methods in Atmospheric Models,* Vol. 1, Reading, United Kingdom, ECMWF, 103–117.

Tung, K. K., 1983: Initial value problem for Rossby waves in a shear flow with critical level. *J. Fluid Mech.,* **133,** 443–469.

Zhang, Z., 1988: The linear study of zonally asymmetric barotropic flows. Ph.D. dissertation, University of Reading, 178 pp.